

The multiple solutions of self-consistency condition in Walecka model and the validity of the Brown-Rho scaling law

Zhang Benwei, Hou Defu and Li Jiarong

Institute of Particle Physics, Hua-Zhong Normal University, Wuhan 430079, China

Abstract

We investigate the self-consistency condition (SCC) of mean-field theory in Walecka model and find that the solutions of the SCC are multiple at high temperature and chemical potential. Using the effective Lagrangian approach, we study medium effects on the ω meson mass by taking into account of vacuum effects. We show that the ω meson mass decreases with both temperature and chemical potential with a general tendency, while near the critical point several ω meson masses become degenerate due to the multiple solutions of the SCC. We check the validity of Brown-Rho scaling law in this case. Finally, we calculate the thermodynamic potential and prove that the multiple solutions of the SCC result from a first-order phase transition of nuclear matter in the Walecka model at high temperature and chemical potential.

PACS numbers: 21.65. +f, 14.40. Cs, 11.10. Wx

Typeset using REVTeX

Investigations of how the properties of hadrons are modified at high temperature and/or density have attracted a lot of attention recently[1-12,16]. This studies can help us to better understand the properties of the chiral phase transition and the quark-gluon plasma which is expected to be created in relativistic heavy ion collisions. One of the most interesting issues concerns the vector meson masses in medium. The dependence of vector meson properties on the temperature and/or the density of the nuclear medium is far from being well understood. There are still a lot of controversies: the results obtained by different methods do not coincide. Some authors [3,4] find the vector meson masses decrease with temperature and/or density which is interpreted as evidence of the partial restoration of chiral symmetry [5,6]. For example, with effective chiral Lagrangians and a suitable incorporation of the scaling property of QCD, it has been shown [1] that the effective masses of σ, ρ, ω mesons and nucleons satisfy the approximate in-medium scaling law

$$\frac{m_\sigma^*}{m_\sigma} \approx \frac{m_\rho^*}{m_\rho} \approx \frac{m_\omega^*}{m_\omega} \approx \frac{m_N^*}{m_N}. \quad (1)$$

Incontrast, others [7,8] have proven that the vector meson masses increase in hot and/or dense matter by using effective theories. In addition,, because the vacuum structure in hot and/or dense medium is changed, the vacuum effect on the vector meson masses should be taken into account [1,9-12]. Using this idea some authors[10-12] calculate the vector meson masses also by using the effective langrangian approach and find the vector meson masses are reduced at either finite temperature or density. In order to include the vacuum effect in medium, some calculations use the Walecka model to get the effective nucleon mass M^* from the self-consistent condition (SCC) $M^* = M - g_s\phi$ by using mean-field theory (MFT). One obtains a single solution M^* in all regions of the parameter space. In this paper we perform a careful and detailed investigation of these issues and find some new results. We first study the SCC in MFT of the Walecka model and find the solutions of the SCC are multiple for some values of the thermodynamic parameters. Then we investigate the ω meson mass in hot and dense matter within the imagine time formalism of finite temperature field theory. We consider an ωNN interaction and include vacuum effects . We show that the ω meson

mass decreases with both temperature and chemical potential with an overall tendency, while multiple ω meson masses become degenerate at some values of the temperature and the chemical potential. Finally we use our concrete numerical results to check the Brown-Rho scaling law Eq.(1) at different temperatures and chemical potentials and give a physical interpretation for the multiple solutions in terms of the thermodynamic potential.

We begin by using the Walecka model (often called QHD-I) [13] to get the changes of the nucleon mass at finite temperature and density. The Lagrangian density in the Walecka model is given by

$$\begin{aligned} \mathcal{L} = & \bar{\psi}[\gamma_{\mu}(i\partial^{\mu} - g_{\nu}V^{\mu}) - (M - g_s\phi)]\psi + \frac{1}{2}(\partial_{\mu}\phi\partial^{\mu}\phi - m_s^2\phi^2) \\ & - \frac{1}{4}F_{\mu\nu}F^{\mu\nu} + \frac{1}{2}m_v^2V_{\mu}V^{\mu} + \delta\mathcal{L}, \end{aligned}$$

which contains fields for baryons $p, n(\psi)$, the neutral scalar meson $\sigma(\phi)$ and the vector meson $\omega(V_{\mu})$. From mean-field theory(MFT)[14], the self-consistency condition(SCC) can be derived as

$$M^* = M - g_s\phi = M - \frac{g_s^2}{m_s^2} \frac{2}{\pi^2} \int p^2 dp \frac{M^*}{\omega_N^*} [n_p(T) + \bar{n}_p(T)], \quad (2)$$

where M^* is the nucleon effective mass and

$$n_p(T) = \frac{1}{e^{\beta(\omega_N^* - \mu)} + 1}, \quad \bar{n}_p(T) = \frac{1}{e^{\beta(\omega_N^* + \mu)} + 1}, \quad \omega_N^* = \sqrt{p^2 + M^{*2}}, \quad \beta = \frac{1}{T}.$$

This expression indicates that the main contribution to the reduction of M^* comes from the effect of the scalar σ meson. Taking the parameters [14] $g_s^2 = 109.626$ and $m_s = 520$ MeV, we can get the nucleon effective mass M^* by numerically solving Eq.(2). The results are depicted in Fig. 2 to Fig. 6. We can see that M^* decreases with temperature T and chemical potential μ , and when T and μ are not very large there is only one solution of the SCC. However, as T and μ become larger there appear three different solutions for the nucleon effective mass. In Fig. 2 we show the dependence of M^* on the temperature T when the chemical potential $\mu = 0$. There are three solutions for M^* when T ranges from 185.7 MeV to 186.6 MeV. This very narrow range was ignored in the previous literature and

consequently all previous calculations obtained a single solution of the SCC for M^* ¹. In Fig. 3 we draw the multiple solutions for M^* in detail in the range and we can easily see the three different solutions for M^* in this range. For example, when $T = 185.8$ MeV we get $M^* = 390.49$ MeV, $M^* = 455.813$ MeV or $M^* = 683.377$ MeV as the solutions of the SCC. When $T = 186.4$ MeV we get $M^* = 352.134$ MeV, $M^* = 534.399$ MeV, $M^* = 648.193$ MeV. From Fig. 4 and Fig. 5 we find the same phenomenon in the dependence of M^* on T when $\mu = 200$ MeV, but the parameter range corresponding to multiple solutions enlarges to nearly 7 MeV. In Fig. 6 we show the μ dependence of M^* when $T = 100$ MeV. We find the three solutions appear in a large range of nearly 200 MeV.

Next we turn to study the ω meson effective mass in hot and dense matter. In Minkowski space the self-energy can be generally expressed as

$$\Pi^{\mu\nu} = F P_L^{\mu\nu} + G P_T^{\mu\nu}, \quad (3)$$

where $P_L^{\mu\nu}$ and $P_T^{\mu\nu}$ are standard longitudinal and transverse projection tensors respectively, and are defined as

$$P_T^{00} = P_T^{0i} = P_T^{i0} = 0, P_T^{ij} = \delta^{ij} - \frac{k^i k^j}{\mathbf{k}^2}, P_L^{\mu\nu} = \frac{k^\mu k^\nu}{k^2} - g^{\mu\nu} - P_T^{\mu\nu}. \quad (4)$$

The full propagator of the ω meson reads

$$\mathcal{D}^{\mu\nu} = -\frac{P_L^{\mu\nu}}{k^2 - m_\omega^2 - F} - \frac{P_T^{\mu\nu}}{k^2 - m_\omega^2 - G} - \frac{k^\mu k^\nu}{m_\omega^2 k^2}. \quad (5)$$

By making use of Eqs.(3) and (4), one can show

$$F(k) = \frac{k^2}{\mathbf{k}^2} \Pi^{00}(k), \quad G(k) = -\frac{1}{2} [\Pi_i^i + \frac{k_0^2}{\mathbf{k}^2} \Pi^{00}(k)]. \quad (6)$$

In order to get the effective mass of the ω meson, we take the limit $\mathbf{k} \rightarrow 0$, and show that $F = G$ and $k^2 = k_0^2 - \mathbf{k}^2 = \omega^2$. The effective mass of the ω meson in hot and dense medium is obtained from the pole of the full propagator

¹Serot[14] once speculated that there might be several solutions of SCC for fixed T and μ , but he did not give concrete and affirmative results.

$$\omega^2 - m_\omega^2 - \text{Re}[\lim_{\mathbf{k} \rightarrow 0} F(k)] = 0. \quad (7)$$

The Lagrangian density for ωNN interaction reads

$$\mathcal{L}_I = g_{\omega NN} \bar{\psi} \gamma_\mu \omega^\mu \psi, \quad (8)$$

where ω^μ and ψ are the ω meson and nuclear fields respectively. Using the imaginary-time formalism of the finite temperature field theory, one can obtain the self-energy for the ω meson (Fig.1)

$$\Pi_\rho^{\mu\nu} = 2g_{\rho NN}^2 T \sum_{n=-\infty}^{+\infty} \int \frac{d^3 p}{2\pi^3} T r [\gamma_\mu(k) \frac{1}{\gamma^s p_s - M^*} \gamma_\nu(-k) \frac{1}{\gamma^s(p_s - k_s) - M^*}], \quad (9)$$

with $p_0 = (2n + 1)\pi T i + \mu$, $k_0 = 2l\pi T i$. By making use of the mathematical expression

$$T \sum f(p_0 = (2n + 1)\pi T i + \mu) = \frac{T}{2\pi i} \oint dp_0 f(p_0) \frac{1}{2} \beta \tanh[\frac{1}{2} \beta(p_0 - \mu)],$$

one can separate the vacuum contributions from the matter contributions [15]:

$$T \sum f(p_0 = (2n + 1)\pi T i + \mu) = -\frac{1}{2\pi i} \int_{-i\infty+\mu+\epsilon}^{+i\infty+\mu+\epsilon} dp_0 f(p_0) \frac{1}{e^{\beta(p_0-\mu)} + 1} - \frac{1}{2\pi i} \int_{-i\infty+\mu-\epsilon}^{+i\infty+\mu-\epsilon} dp_0 f(p_0) \frac{1}{e^{-\beta(p_0-\mu)} + 1} + \frac{1}{2\pi i} \int_{-i\infty}^{+i\infty} dp_0 f(p_0 - \mu).$$

The first two terms correspond to matter contributions as functions of temperature and chemical potential, while the last term accounts for vacuum contributions.

The last term is divergent. Using dimensional regularization to get rid of the divergence, we obtain from Eq.(7)

$$\Pi_{vac}^{\mu\nu}(k) = \frac{g_{\omega NN}^2}{\pi^2} (k^\mu k^\nu - k^2 g^{\mu\nu}) \omega^2 \int_0^1 dz z(1-z) \ln \left[\frac{M^{*2} - \omega^2 z(1-z)}{M^2 - m_\omega^2 z(1-z)} \right]. \quad (10)$$

Using the residue theorem and the periodicity condition of k_0 in the finite temperature field theory[15], we can then get the matter contribution,

$$\begin{aligned} \Pi_{mat}^{00}(k) = & -\frac{g_{\omega NN}^2}{\pi^2} \int dp \frac{p^2}{\omega_N^*} [n_p(T) + \bar{n}_p(T)] \\ & [2 + \frac{4\omega_N^* k^0 - 4\omega_N^{*2} - k^2}{4p|\mathbf{k}|} \ln \frac{k^2 - 2k^0 \omega_N^* + 2p|\mathbf{k}|}{k^2 - 2k^0 \omega_N^* - 2p|\mathbf{k}|}] \end{aligned}$$

$$\begin{aligned}
& + \frac{-4\omega_N^* k^0 - 4\omega_N^{*2} - k^2}{4p|\mathbf{k}|} \ln \frac{k^2 + 2k^0\omega_N^* + 2p|\mathbf{k}|}{k^2 + 2k^0\omega_N^* - 2p|\mathbf{k}|}, \\
(\Pi_i^i(k))_{mat} = & -2\frac{g_{\omega NN}^2}{\pi^2} \int dp \frac{p^2}{\omega_N^*} [n_p(T) + \bar{n}_p(T)] \\
& [2 - \frac{2M^* + k^2}{4p|\mathbf{k}|} (\ln \frac{k^2 - 2k^0\omega_N^* + 2p|\mathbf{k}|}{k^2 - 2k^0\omega_N^* - 2p|\mathbf{k}|} \\
& + \ln \frac{k^2 + 2k^0\omega_N^* + 2p|\mathbf{k}|}{k^2 + 2k^0\omega_N^* - 2p|\mathbf{k}|})],
\end{aligned}$$

where $\omega_N^* > \mu$. From Eq.(7) we can obtain $F(k)$ and $G(k)$ which allow us to study the dependence of m_ω on the momentum \mathbf{k} . However, we are interested here in the effective mass of the ω meson, thus we take the limit $\mathbf{k} \rightarrow 0$ and find

$$\text{Re}[\lim_{\mathbf{k} \rightarrow 0} F_{vac}(k)] = \frac{g_{\rho NN}^2}{\pi^2} \omega^2 \int_0^1 dz z(1-z) \ln \left[\frac{M^{*2} - \omega^2 z(1-z)}{M^2 - m_\omega^2 z(1-z)} \right], \quad (11)$$

$$\begin{aligned}
\text{Re}[\lim_{\mathbf{k} \rightarrow 0} F_{mat}(k)] = & -\frac{4g_{\rho NN}^2}{\pi^2} \int p^2 dp \frac{1}{\omega_N^*(\omega^2 - 4\omega_N^{*2})} \\
& \left[\frac{1}{e^{\beta(\omega_N^* + \mu)} + 1} + \frac{1}{e^{\beta(\omega_N^* - \mu)} + 1} \right] \left(\frac{4}{3} p^2 + 2M^{*2} \right). \quad (12)
\end{aligned}$$

Note that ωNN interaction will affect M^* . However, as has been pointed out by other authors [16], the effects due to vector meson exchange upon M^* are very small and can be neglected. This procedure is consistent with our treatment of the nucleon mass M^* since M^* is determined only by the scalar and fermion fields within the Walecka model in MFT, and there will be no effect on M^* from vector mesons

With M^* given by Eq.(2) we can solve Eq.(7) numerically and determine the modified meson mass m_ω^* as a function of temperature and chemical potential. We choose a coupling of $\frac{g_{\omega NN}^2}{4\pi} = 20.0$ [17]. In Fig. 2 to Fig.5 we show the temperature dependences of the ω meson mass at $\mu = 0$ and $\mu = 200$ MeV respectively and find that the ω meson mass decreases with temperature with an overall tendency. Fig.6 shows the chemical potential dependence of the ω meson mass at $T = 100$ MeV. The ω meson mass also decreases with increasing chemical potential μ with a general tendency, which is consistent with the result by other authors [18]. However, in contrast to the results of other authors we find that for high T and/or μ there may be several solutions for ω meson masses. Using our results we can check the

Brown-Rho scaling law Eq. (1). We draw the curves of the T and μ dependences of $\frac{M_N^*}{M_N}$ and $\frac{m_\omega^*}{m_\omega}$ in figures from Fig.2 to Fig.6 We find that the scaling law works well when T and μ are not too high and there is a single solutions for M^* and m_ω^* . But when the temperature and chemical potential are large , the scaling law will be broken, since there are several different solutions for M^* and m_ω^* .

In order to get deeper insight into the multiple solutions of the SCC, we calculate the thermodynamic potential for Walecka Model [19],

$$\Omega = \frac{1}{2}(m_s^2\phi^2 + m_v^2\mathbf{V}^2 - m_v^2V_0^2)V - T \sum_{\mathbf{p},\lambda} [\ln(1 + e^{-\beta(\omega_N^* - \mu)}) + \ln(1 + e^{-\beta(\omega_N^* + \mu)})]$$

In this expression, the sums run over all single-particle states labelled by momenta \mathbf{p} and intrinsic quantum number λ . From the thermodynamic potential one can obtain all of the thermodynamic functions. As shown in Fig. 7, from the isotherms of the thermodynamic potential as a function of M^* , we find that when T is not too high, the thermodynamic potential only has one extreme point, but as T increases to near 186 MeV, there are three extreme points, which correspond with the three solutions for M^* . Furthermore, when T continues to increase, there is again only one extreme point . The amplified region where the thermodynamic potential has three extreme points is depicted more clearly in Fig. 8. In Fig. 9 we show the phase diagram of nuclear matter in the Walecka model. This diagram looks quite similar to the Van Der Waals isotherm of gas-liquid transitions. Figures from Fig. 7 to Fig. 9 indicate explicitly that nuclear matter described by Walecka model has a first-order phase transition at high temperature and density, which results in the multiple solutions for the nucleon and omega meson masses.

In summary, we have studied the nucleon effective mass within the Walecka model in the imaginary time formalism of finite temperature field theory. Within the effective Lagrangian approach we investigate the medium effects on the ω meson mass and include the vacuum effects. We show that m_ω^* decreases with both temperature and chemical potential with an overall tendency. From the thermodynamic potential and the phase diagram we find

that Walecka model in MFT predicts a first-order phase transition at high temperature and chemical potential, which consequently leads to multiple solutions for M^* and m_ω^* which results in the breaking of the Brown-Rho scaling law. Of course our results may depend on the model and might only occur within the mean-field approximation. It would be interesting to extend this work to other models and to go beyond MFT. In this paper we have only discussed the ω meson effective mass in medium, but our discussions can also be applied to the ρ meson mass in hot and/or dense matter and we expect similar results will be obtained.

ACKNOWLEDGMENTS

We are grateful to M. E. Carrington for a careful reading of the manuscript. This work was supported in part by the National Natural Science Foundation of China (NSFC) under Grant No.(19775017)

REFERENCES

- [1] G. E. Brown and M. Rho, Phys. Rev. Lett 66(1991) 2720.
- [2] V. L. Eletsky, B. L. Ioffe, Phys. Rev. Lett. 78(1997)1010.
- [3] T. Hatsuda and S. H. Lee, Phys. Rev. C46(1992)34.
- [4] M. Asakawa and C. M. Ko, Nucl. Phys. A572(1994)732.
- [5] G. E. Brown, *et al* Phys. Rev. Lett. 60(1988)2723.
- [6] K. Kubodera and M. Rho, Phys. Rev. Lett. 67(1991)3479.
- [7] C. Gale and J. I. Kapusta, Nucl. Phys. B357(1991)65.
- [8] A. Hosaka, Phys. Lett. B244(1990)363.
- [9] A. Mishra, *et al*. Phys. Rev. C56(1997)1380.
- [10] Chungsik Song, *et al*. Phys. Rev. C52(1995)408.
- [11] H. C. Jean, *et al*. Phys. Rev. C49(1994)1981.
- [12] H. Shiomo, T. Hatsuda, Phys. Lett. B334(1994)281.
- [13] J. D. Walecka, Ann. Phys. 83(1974)491.
- [14] B. D. Serot, Rep. Prog. Phys. 55(1992)1855.
- [15] J.I. Kapusta, *Finite Temperature Field Theory*, Cambridge University Press(1989).
- [16] Y.J.Zhang, *et al*. Phys. Rev. C 56(1997)3336, Ping Wang, *et al. ibid.* 59(1999)928.
- [17] R.Machleidt, *et al*. Phys. Rep. 149(1987)1.
- [18] P. Maris, *et al*. Phys. Rev. C57(1998)2821.
- [19] R.J.Furnstahl, B.D.Serot *et al*. Phys. Rev. C43(1991)105.

Figure Captions

Fig. 1 One-loop diagram for ω meson self-energy in the ωNN interaction.

Fig. 2 The temperature dependence of $\frac{M_N^*}{M_N}$ and $\frac{m_\omega^*}{m_\omega}$ at $\mu = 0$ when there is a single solution for M^* and m_ω^* . The solid line represents $\frac{M_N^*}{M_N}$ and the dashed line represents $\frac{m_\omega^*}{m_\omega}$. When $T \sim 186$ MeV each line has a cut, which means there are multiple solutions for M^* and m_ω^* .

Fig. 3 The temperature dependence of $\frac{M_N^*}{M_N}$ and $\frac{m_\omega^*}{m_\omega}$ at $\mu = 0$ in the range 185.7 MeV to 186.6 MeV where multiple solutions for M^* and m_ω^* exist. The solid line represents $\frac{M_N^*}{M_N}$ and the dashed line represents $\frac{m_\omega^*}{m_\omega}$.

Fig. 4 The temperature dependence of $\frac{M_N^*}{M_N}$ and $\frac{m_\omega^*}{m_\omega}$ at $\mu = 200$ MeV where there is a single solution for M^* and m_ω^* . The solid line represents $\frac{M_N^*}{M_N}$ and the dashed line represents $\frac{m_\omega^*}{m_\omega}$.

Fig. 5 The temperature dependence of $\frac{M_N^*}{M_N}$ and $\frac{m_\omega^*}{m_\omega}$ at $\mu = 200$ MeV where there appear several solutions for M^* and m_ω^* and T ranges from 159 MeV to 166 MeV. The solid line represents $\frac{M_N^*}{M_N}$ and the dashed line represents $\frac{m_\omega^*}{m_\omega}$.

Fig. 6 The chemical potential dependence of $\frac{M_N^*}{M_N}$ and $\frac{m_\omega^*}{m_\omega}$ at $T = 100$ MeV. The solid line represents $\frac{M_N^*}{M_N}$ and the dashed line represents $\frac{m_\omega^*}{m_\omega}$.

Fig. 7 The isotherms of the thermodynamic potential as a function of M^* at $\mu = 0$. From top to bottom the five lines represent the isotherms of the thermodynamic potential at $T = 180$ MeV, 185 MeV, 186 MeV, 186.3 MeV and 188 MeV respectively.

Fig. 8 An enlargement of the isotherms of the thermodynamic potential Ω at $\mu = 0$ when Ω has three extreme points at $T \sim 186$ MeV.

Fig. 9 The phase diagram in nuclear matter: pressure as a function of proper volume/baryon for $T = 100$ MeV. The dashed line is Maxwell isotherm.

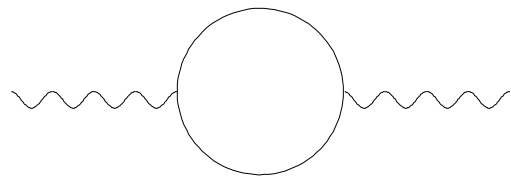


Fig 1.

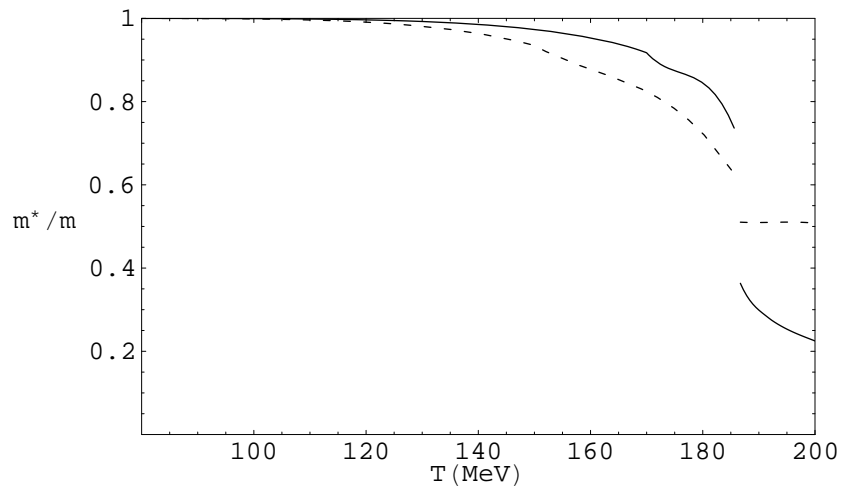


Fig 2.

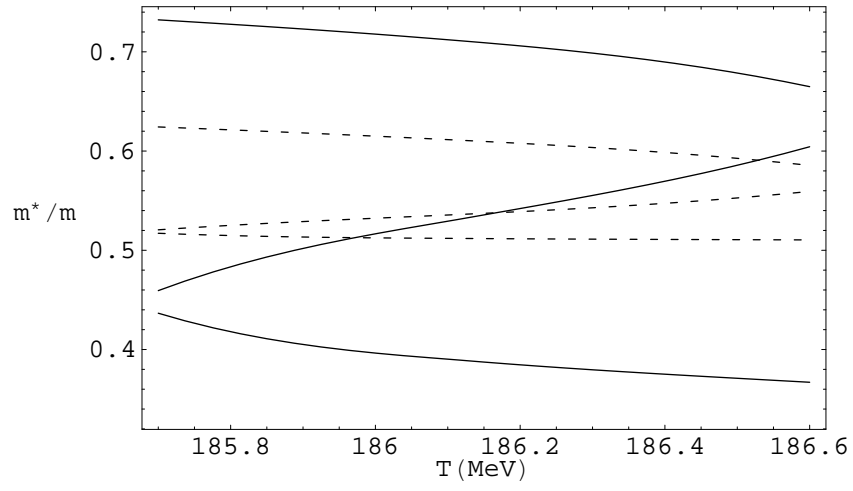


Fig 3.

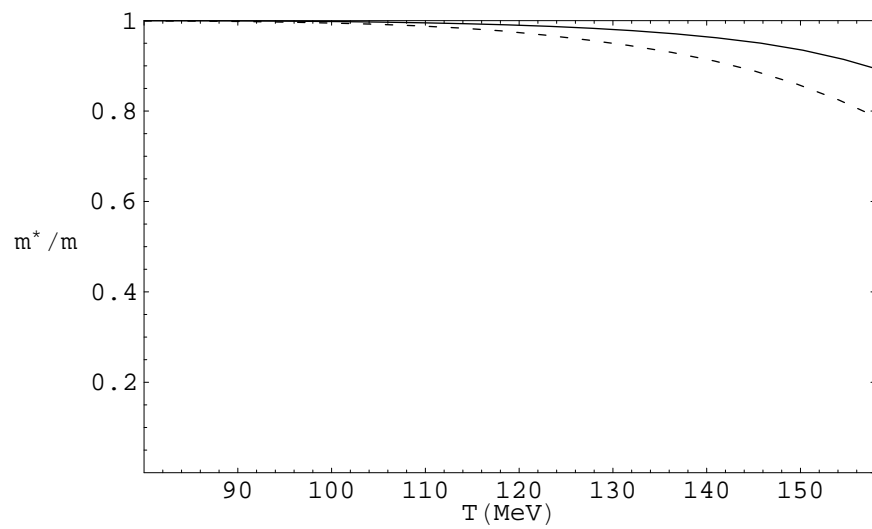


Fig 4.

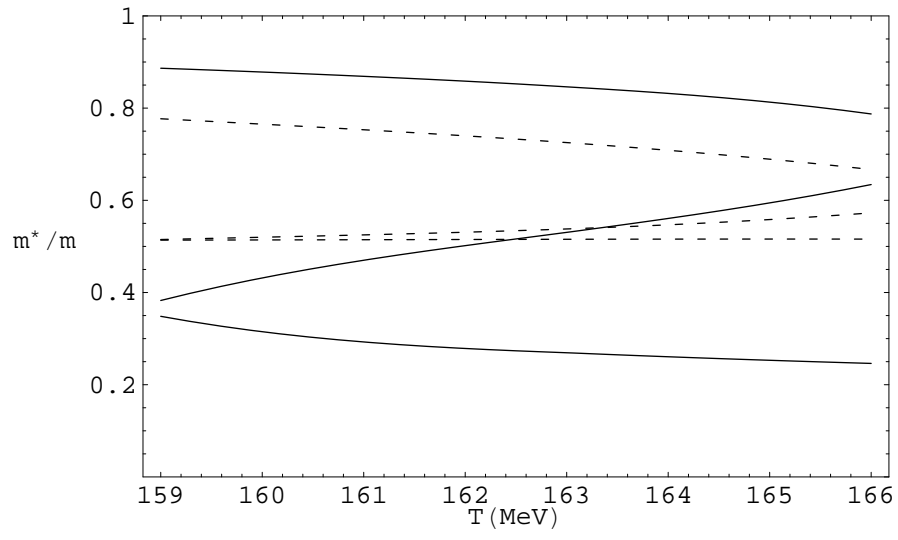


Fig 5.

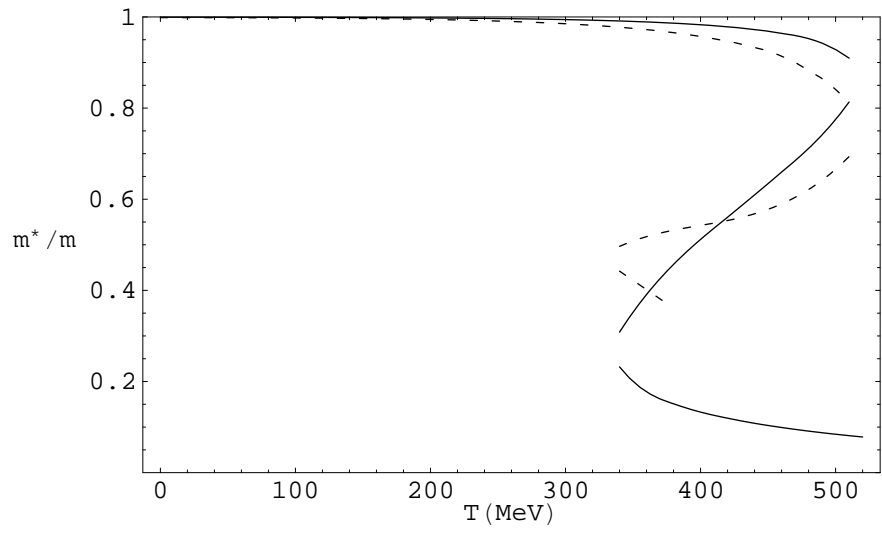


Fig 6.

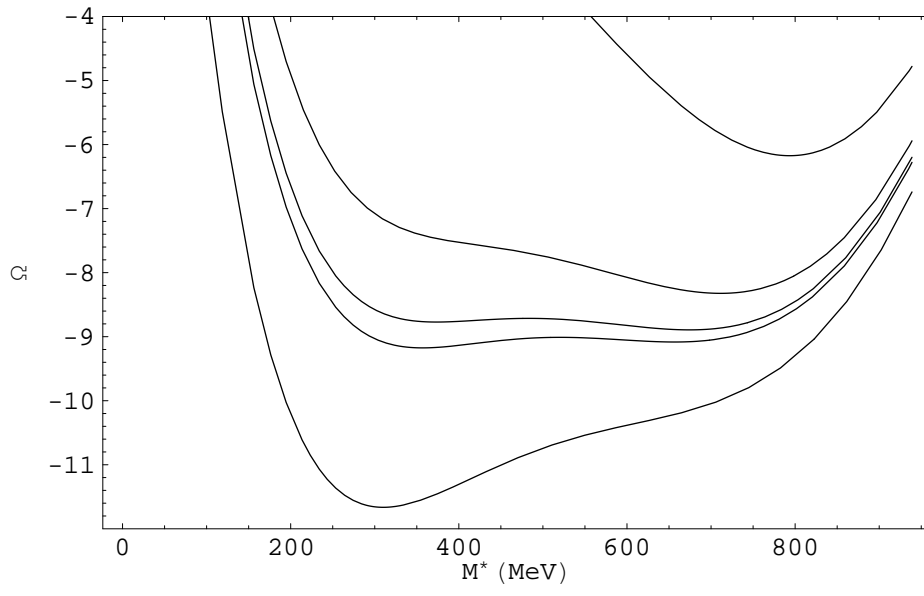


Fig . 7

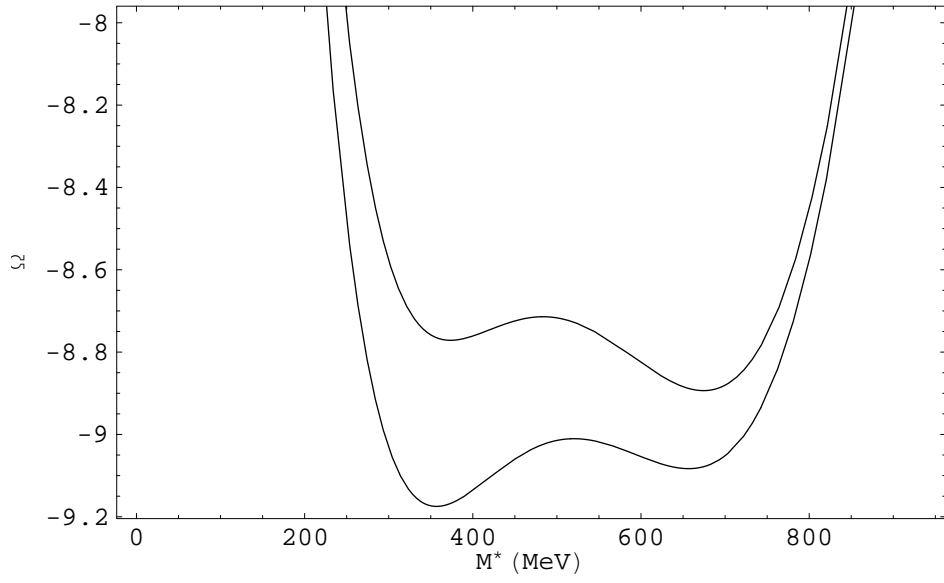


Fig. 8

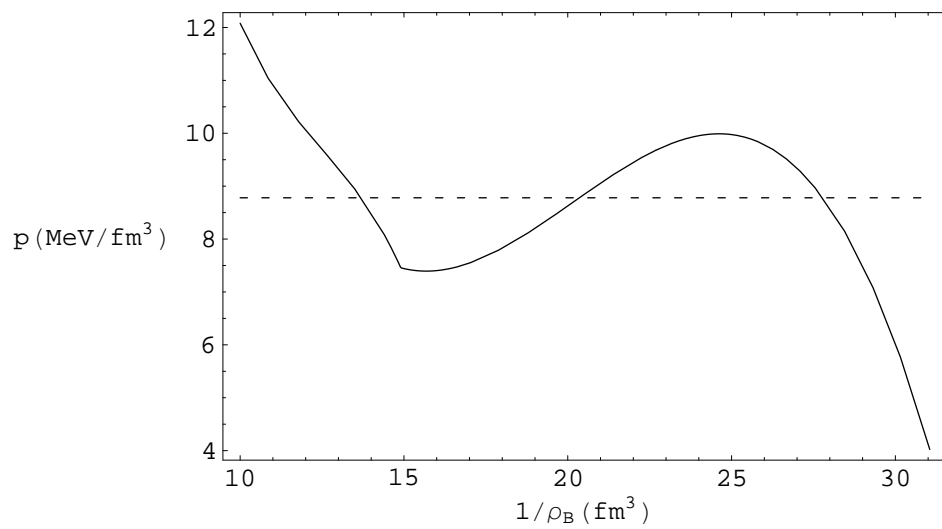


Fig. 9